ACS Photonics

Letter

pubs.acs.org/journal/apchd5

Enhancing Guided Second-Harmonic Light in Lithium Niobate Nanowires

Anton Sergeyev,*,† Reinhard Geiss,‡ Alexander S. Solntsev,§ Andrey A. Sukhorukov,§ Frank Schrempel,‡ Thomas Pertsch,‡ and Rachel Grange†

†Optical Nanomaterial Group, Institute for Quantum Electronics, Department of Physics, ETH Zurich, August-Piccard-Hof 1, 8093 Zurich, Switzerland

‡Institute of Applied Physics, Abbe Center of Photonics, Friedrich Schiller University, Max-Wien-Platz 1, 07743 Jena, Germany

§Nonlinear Physics Center, Research School of Physics and Engineering, Australian National University, Canberra, ACT 0200, Australia

Supporting Information

ABSTRACT: We experimentally demonstrate practical approaches to enhance second-harmonic (SH) generation in individual lithium niobate nanowires (NWs) with a submicrometer cross-section and length up to tens of micrometers. We establish that parametric interactions of guided modes propagating along the NW determine the SH output power, which can be therefore controlled by the NW length. We show that the SH power is increased by about 84 times at wavelengths corresponding to modal phase-matching. Importantly, at non-phase-matched wavelengths the SH power can be improved by a factor of up to 9.3 by adjusting the NW length with a focused ion beam. We also characterize SH emission directionality, which can be further tailored for applications in integrated optical circuits and nonlinear microscopy.

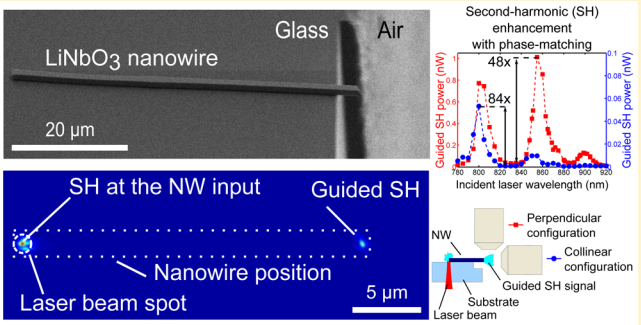

KEYWORDS: *nanowire, lithium niobate, second-harmonic generation, phase-matching, focused ion beam*

The ability of nanowires (NWs) to guide light makes them valuable for miniaturizing optical devices and developing sophisticated nanoscale applications. For instance, NWs can be used for transporting light within an optical chip,[1,2] for providing laser irradiation,[3−5] and for localized imaging.[6] However, the NW applications can be further developed if the wave-guiding properties of NWs are combined with nonlinear optics effects, such as second-harmonic generation (SHG) or sum-frequency generation. Indeed, the NWs made from nonlinear material have already been applied as nonlinear optical sources[7−9] and subwavelength microscopy probes.[10]

Along with widely studied semiconductor NWs,[11−13] chemically synthesized[14] and lithographically fabricated[15] lithium niobate ($LiNbO_3$) NWs have been shown to generate and guide the second-harmonic (SH). In addition, we have also demonstrated efficient dye excitation with the guided SH in $LiNbO_3$ NWs.[15] However, the small size of NWs limits the SHG efficiency due to its quadratic dependence on volume.[16,17] Consequently, optimization of the SHG efficiency is necessary to obtain powerful nanoscale devices. To increase the SH signal, one can apply plasmonic resonances[18−20] or phase-matching.[21−23] The first method is applied to subwavelength nanoscale structures, where phase-matching does not take place but the SH intensity is still low due to small material volume.[18,19] The second one is well known for bulk material and has been the focus of many research works to develop waveguides,[24,25] optical parametric oscillators,[26,27] and resonators[28] in $LiNbO_3$ crystals. The phase-matching effect is widely studied in large waveguides with typical cross-sections of several micrometers.[24] Nevertheless, it has not been studied experimentally in NWs with cross-sections of hundreds of nanometers, which is the typical size of future devices for integrated optics.[29]

In this work, we study $LiNbO_3$ NWs that are produced through a top-down fabrication method with typical cross-section dimensions of 550×780 nm^2 and lengths up to 52 μm. We will use modal phase-matching to demonstrate the origin of the SH signal and consolidate our results with corresponding simulations. We will also show that different guided SH modes scatter differently out of the NW, and this has consequences on the directionality of the light for further applications. Finally, we will show that we can control and increase the non-phase-matched SHG by optimizing the NW length with focused-ion-beam (FIB) milling.

The $LiNbO_3$ NWs are fabricated with a top-down method called ion-beam enhanced etching.[15,30] This method employs argon and helium ion irradiation to amorphize specified regions

Received: March 16, 2015
Published: June 3, 2015

DOI: 10.1021/acsphotonics.5b00126
ACS Photonics 2015, 2, 687−691

of an x-cut $LiNbO_3$ wafer both on the surface and in depth. The amorphized wafer regions lose chemical stability and are removed by wet etching in hydrofluoric acid. As a result, we obtain free-lying $LiNbO_3$ NWs on the crystal substrate. The NWs keep the crystal structure of the wafer. Thus, crystal axes are parallel to the geometrical axes of a NW as shown in the inset of Figure 1.

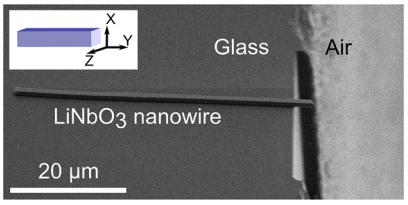

Figure 1. SEM image of an individual $LiNbO_3$ NW on an ITO-coated glass slide. The NW is brought close to the edge of the substrate so that one of its ends is suspended in air. Inset: Crystal structure of the $LiNbO_3$ NW.

For the experiment, we transfer a NW off the substrate onto a glass slide with an indium tin oxide coating by means of a micromanipulator in a scanning electron microscope (SEM). We position the NW so that its output facet protrudes from the glass slide's edge by about 3.4 μm (Figure 1). Such positioning of the NW enables imaging of the NW output facet with a long working distance objective. We find it important to mention that both NW facets are cut perpendicularly to the NW length with a FIB. The values of the NW's height of 541 ± 27 nm, width of 778 ± 38 nm, and length of 52 ± 2 μm are obtained by an SEM. The inaccuracy is caused by the resolution and contrast limits of the SEM images.

We use a Ti:sapphire laser source with a pulse repetition rate of 80 MHz and a pulse duration of 295 fs at the central wavelength of 820 nm. The experimental setup consists of focusing and detecting parts (Figure 2a). The focusing part includes a half-wave plate to rotate the linear polarization, a 20× objective to focus the laser beam onto an end of a NW

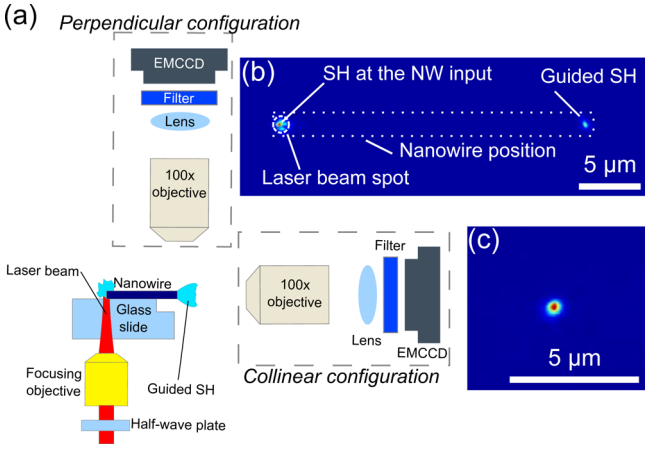

Figure 2. (a) Schematics of the used experimental setup with both the collinear and perpendicular detection configurations. (b) Typical SH response of a $LiNbO_3$ NW collected in the perpendicular configuration. The SH at the illuminated facet is generated by the focused laser beam. The signal at the opposite NW end is the guided SH. (c) Image of the guided SH obtained in the collinear configuration.

perpendicularly to the sample plane, and a 3D translation stage to optimize the NW position within the beamspot. The detecting part consists of a 100× objective (with a numerical aperture of 0.75 and working distance of 4 mm), a lens, and an electron-multiplying charge-coupled-device (EMCCD) camera.

The detecting part can be positioned either collinearly or perpendicularly to the NW. In the perpendicular configuration, the detecting part is placed at 90° with respect to the NW and is imaging the whole NW (Figure 2b). In the collinear configuration, the detecting part is in line with the NW and is imaging its output facet (Figure 2c). Using both configurations allows us to study the spatial distribution of the guided SH signal.

To detect the SH response, we focus the laser beam on a NW facet and filter out the laser light with a bandpass filter at the camera position. In Figure 2b, we show a typical SH response of a NW. The SH at the illuminated facet is generated by the focused laser beam. The signal at the opposite NW end is the SH that is guided inside the NW. Even though we have already demonstrated that the generated SH can be guided in $LiNbO_3$ NWs,[15] it is not clear where exactly in the NW the SHG process takes place. On one hand, the guided SH may be a fraction of the SH light that is generated by the incident laser beam at the NW input facet and scattered into the SH waveguide modes. On the other hand, the incident laser light may be scattered into the guided modes of a so-called fundamental harmonic (FH) that generates the SH inside the NW. By clearing up this point, we will be able to control and increase the SHG efficiency in NWs.

Aiming to determine the origin of the guided SH, we check the dependence of the guided SH power on the laser wavelength. For this purpose, we change the central wavelength from 780 nm up to 920 nm with a 5 nm step and measure the guided SH power. In addition, the measurement is performed in both collinear and perpendicular detecting configurations to study the spatial distribution of the guided SH. The average laser power was kept at 3.4 mW at the sample position, and the laser beamspot diameter at focus was about 1.2 μm. The laser polarization was set to 20° with respect to the nanowire length throughout the experiments in both configurations. At this polarization, the guided SH power was maximal. However, the polarization at which the maximum SH signal is obtained varies for each NW probably because of the shape and size of the NW input facet.

Figure 3 displays the guided SH power versus the incident laser wavelength for collinear and perpendicular collection configurations. Both plots reveal several peaks with enhancement factors up to 84 and 48 for collinear and perpendicular configurations, respectively. These peaks follow the shape of a sinc function and, therefore, indicate the phase-matching mechanism.[16] In NWs, the phase-matching mechanism matches effective refractive indices of the guided FH and SH modes. Thus, the observed peaks in Figure 3 indicate the presence of the guided modes. It allows us to conclude that the guided SH is not the scattered SH from the input, but it is excited by the FH guided modes of the laser light inside the NW. In addition, the presence of multiple peaks indicates phase-matching of multiple pairs of the FH and SH guided modes. Thus, the NWs give more freedom in choosing a wavelength for phase-matching without any need for other tuning mechanisms such as temperature tuning.[16]

Comparing both curves in Figure 3, one can also see differences in the guided SH power values collected in both

DOI: 10.1021/acsphotonics.5b00126
ACS Photonics 2015, 2, 687−691

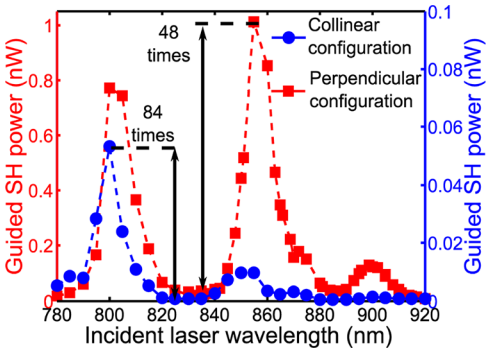

Figure 3. Guided SH power collected in the collinear (blue circles) and perpendicular (red squares) detecting configurations versus the incident laser wavelength. The dashed lines are included to guide the eye.

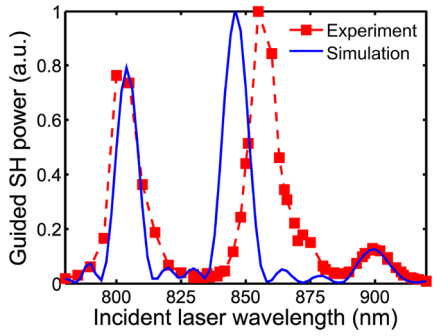

Figure 4. Experiment (red squares) and the simulation results for a NW with a height of 560 nm and width of 778 nm (blue solid curve). The dashed line is added to guide the eye. The simulation curve includes contributions from the first three FH modes and 30 SH modes. The contributions of only three mode pairs are relevant since the other mode pairs show low conversion efficiency.

detecting configurations. First, the SH power in the perpendicular configuration (red squares) exceeds the SH power in the collinear one (blue circles) by 14.5 times at λ = 800 nm, by 100 times at λ = 855 nm, and by 91 times at λ = 900 nm. Second, the relative heights of the peaks vary when the detecting configuration is changed. When the guided SH is collected in the collinear configuration (blue circles), the peak at λ = 800 nm is dominant and the peak at λ = 900 nm is almost nondistinguishable. In turn, when the guided SH is collected in the perpendicular configuration (red squares), all three peaks are more pronounced and the dominant peak is at λ = 855 nm.

The fact that more light is collected in the perpendicular configuration means that the guided SH is not preferably scattered along the NW length but at a certain angle. Moreover, the change of the relative heights points out that the scattering angle varies for each guided mode. These observations may be caused by a difference in effective refractive indices and the field distributions of the corresponding modes. Besides the difference in the scattering of modes, the shape of the output facet may also influence the scattering direction and distribution of the scattered light. Therefore, we expect that one can engineer a specific radiation pattern of the guided light distribution by modifying the NW output facet[31] and exciting specific guided modes.[12] It may complement NW imaging applications[6,10,15] by defining the area to be irradiated with the guided SH signal.

To confirm theoretically phase-matching in the studied $LiNbO_3$ NW, we have simulated the processes of waveguiding and SHG in the NW.[15,32] The performed simulation finds three FH and 30 SH guided modes and their effective refractive indices using the COMSOL software. Then, we find the conversion efficiency between each FH and SH mode and sum up the conversion efficiencies of all mode pairs to find the total response (see the Supporting Information). For the simulation, we use a $LiNbO_3$ crystal's wavelength-dependent refractive index tensor at the temperature of 23 °C from ref 33, the second-order susceptibility tensor from ref 16, and the crystal structure as shown in the inset of Figure 1. Since the SEM measurement of the studied NW contains an uncertainty, we have performed simulations for several values of width and height within the uncertainty range and a NW length of 52 μm. The simulation shows the best match with the experiment at a height of 560 nm and width of 778 nm. However, the experiment and simulation curves that are plotted in Figure 4 still have a slight lateral discrepancy. One of the possible reasons for the observed discrepancy may be the high order of the involved guided SH modes. Such modes have a large part of their intensity profile outside the NW,[34] and, thus, their effective refractive index may be modified by the NW surface imperfection. Indeed, according to the simulation results, the peak at λ = 802 nm is created by the first FH and 17th SH modes, the peak at λ = 846 nm is created by the third FH and 23th SH modes, and the peak at λ = 900 nm is created by the second FH and 15th SH modes (see the Supporting Information). Note that, due to resolution limits, we cannot resolve the mode pattern, and, therefore, Figure 2c displays a single spot.

In addition, in the model, we have taken into account nonuniform coupling of the laser light into various FH modes. Thus, in the simulation, we have also varied contribution weights of the FH modes to match the heights of the measured and calculated peaks in Figure 4. Nevertheless, we also expect that the height of a specific peak can be increased by coupling more power into the corresponding FH mode. It can be achieved by changing coupling conditions such as shaping the input facet or changing incident laser polarization.[12]

However, at most wavelengths, a NW does not provide any phase-matching of mode pairs of the FH and SH. But it may still provide a mode pair with a high power conversion efficiency that will still contribute significantly to the SHG process inside the NW despite their phase-mismatching.

As an example, we show in Figure 5 the calculated contribution of the first and second FH modes at a wavelength of 820 nm to the SH while being guided inside a NW. In the calculation, we set the NW height, width, and length to 510 nm, 728 nm, and 34 μm, respectively. Both plotted curves in Figure 5 reveal periodic oscillations of the guided SH power along the NW length. These oscillations come from alternating conversion and back-conversion of the SH. Thus, the oscillation period depends on the mismatch of the refractive indices of the FH and SH mode pairs, and the oscillation depth depends on the conversion efficiency of the corresponding FH and SH mode pairs.[16] Therefore, a careful design of the NW length can yield a significant increase of the guided SH power at the output of the NW. In this particular case, the simulation predicts an increase of the guided SH power up to a factor of 6.5 for the first FH mode and of 9.5 for the second FH mode.

Since the overall oscillation period is in a micrometer range, the NW length can be optimized by means of FIB milling. In the following experiment, we demonstrate the possibility of

DOI: 10.1021/acsphotonics.5b00126
ACS Photonics 2015, 2, 687−691

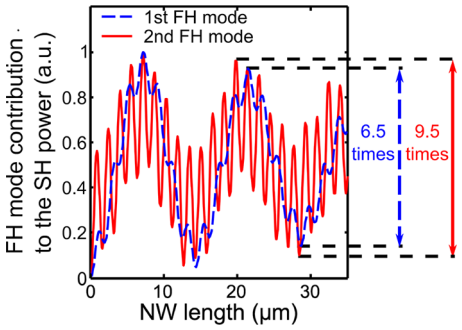

Figure 5. Calculated contribution of the first FH (blue dashed line) and second FH (red solid line) modes to the guided SH power versus NW length. The curves plot the contributions of the first and second FH modes to the SHG process by interacting with 35 SH modes. The total contribution is found by summing up the contribution of each pair of FH and SH modes.

controlling the guided SH power by cutting the NW length with a FIB. For the experiment, we used a NW with a height of 728 ± 36 nm, width of 510 ± 26 nm, and initial length of 34.8 μm as in the simulations of Figure 5. We shortened the NW length in several steps down to 23.6 μm. After each milling procedure, we measured the power of the guided SH. We plot the SH power measured at varied NW length in Figure 6. The

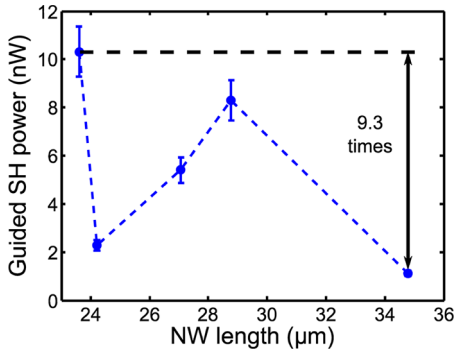

Figure 6. Power of the guided SH versus the NW length after different cuts along the same NW. The dashed line is included to guide the eye.

NW length to be cut varied between 0.61 and 6 μm. Since the output facet shape may have an influence on the guided SH, the facet was cut perpendicularly to the NW length each time to ensure the same light distribution of the guided signal. The laser wavelength was 820 nm, the diameter of the laser beamspot was 4 μm, and the incident laser power was 10 mW at the sample position. The laser polarization was set to 154° with respect to the NW length. For the experiment, we used the perpendicular detecting configuration.

Figure 6 shows that the NW length influences strongly the guided SH power. Thus, after shortening the NW length from 34.8 μm down to 23.6 μm, the guided SH power has increased 9.3 times, which corresponds to the calculations in Figure 5. However, the horizontal position of the oscillation may not fit the experimental data due to the uncertainty of the measurements of the NW cross-section. Therefore, some measured power values might be higher or lower than the simulation.

In order to experimentally maximize the SH power at the output of a given NW by cutting it to the optimal length, one has to precisely determine the position of the NW at which the guided SH is the strongest. This task can be performed by sensing the near-field of the guided SH light along the NW by means of a scanning near-field optical microscope.[35,36]

In conclusion, we have studied the generation and guiding of the SH in $LiNbO_3$ NWs. We have demonstrated modal phase-matching in these NWs. This fact proves that the guided SH is generated by the FH guided modes inside the NWs. Importantly, we have also shown that the guided SH power can be changed by modifying the NW length.

In addition, we have studied the spatial distribution of the guided SH intensity after coupling out of the output facet. We have observed that the guided SH modes do not necessarily scatter along the NW optical axis; instead different guided SH modes show different scattering directions.

With this work, we have shown that enhancing the nonlinear optical signal generated in $LiNbO_3$ NWs is possible either by modal phase-matching or by engineering their length. This is essential for developing efficient miniaturized devices for localized imaging, optical sensing, light transfer, or building blocks for integrated optics.

■ ASSOCIATED CONTENT

Supporting Information

Figures S1−S10 and Tables S1−S2. The Supporting Information is available free of charge on the ACS Publications website at DOI: 10.1021/acsphotonics.5b00126.

■ AUTHOR INFORMATION

Corresponding Author

*E-mail: antons@phys.ethz.ch.

Notes

The authors declare no competing financial interest.

■ ACKNOWLEDGMENTS

The authors thank Dragomir Neshev, Jörg Reinhold, Frank Setzpfandt, Andrea Steinbrück, and Marc Reig for fruitful discussions. This work was financially supported by Carl Zeiss Foundation and the Australian Research Council (Future Fellowship FT100100160 and Discovery Project DP130100135).

■ REFERENCES

(1) Voss, T.; Svacha, G. T.; Mazur, E.; Müller, S.; Ronning, C.; Konjhodzic, D.; Marlow, F. High-Order Waveguide Modes in ZnO Nanowires. *Nano Lett.* **2007**, *7*, 3675−3680.

(2) Pauzauskie, P. J.; Yang, P. Nanowire Photonics. *Mater. Today* **2006**, *9*, 36−45.

(3) Ning, C. Z. Semiconductor Nanolasers. *Phys. Status Solidi B* **2010**, *788*, 774−778.

(4) Pauzauskie, P. J.; Sirbuly, D. J.; Yang, P. Semiconductor Nanowire Ring Resonator Laser. *Phys. Rev. Lett.* **2006**, *96*, 143903.

(5) Der, R. R.; Wille, M.; Geburt, S.; Rensberg, J.; Zhang, M.; Lu, J. G.; Capasso, F.; Buschlinger, R.; Peschel, U.; Ronning, C. Continuous Wave Nanowire Lasing. *Nano Lett.* **2013**, *13*, 3602−3606.

(6) Yan, R.; Park, J.-H.; Choi, Y.; Heo, C.-J.; Yang, S.-M.; Lee, L. P.; Yang, P. Nanowire-Based Single-Cell Endoscopy. *Nat. Nanotechnol.* **2012**, *7*, 191−196.

(7) Barrelet, C. J.; Ee, H.-S.; Kwon, S.-H.; Park, H.-G. Nonlinear Mixing in Nanowire Subwavelength Waveguides. *Nano Lett.* **2011**, *11*, 3022−3025.

(8) Zhang, X.; He, H.; Fan, J.; Gu, C.; Yan, X.; Hu, M.; Zhang, X.; Ren, X.; Wang, C. Sum Frequency Generation in Pure Zinc-Blende GaAs Nanowires. *Opt. Express* **2013**, *21*, 28432.

(9) Solntsev, A. S.; Sukhorukov, A. A.; Neshev, D. N.; Kivshar, Y. S. Spontaneous Parametric Down-Conversion and Quantum Walks in

DOI: 10.1021/acsphotonics.5b00126
ACS Photonics 2015, 2, 687−691

Arrays of Quadratic Nonlinear Waveguides. *Phys. Rev. Lett.* **2012**, *108*, 023601.
(10) Nakayama, Y.; Pauzauskie, P. J.; Radenovic, A.; Onorato, R. M.; Saykally, R. J.; Liphardt, J.; Yang, P. Tunable Nanowire Nonlinear Optical Probe. *Nature* **2007**, *447*, 1098−1102.
(11) Pernice, W. H. P.; Xiong, C.; Schuck, C.; Tang, H. X. Second Harmonic Generation in Phase Matched Aluminum Nitride Waveguides and Micro-Ring Resonators. *Appl. Phys. Lett.* **2012**, *100*, 223501.
(12) Sanatinia, R.; Anand, S.; Swillo, M. Modal Engineering of Second-Harmonic Generation in Single GaP Nanopillars. *Nano Lett.* **2014**, *14*, 5376−5381.
(13) Grange, R.; Brönstrup, G.; Kiometzis, M.; Sergeyev, A.; Richter, J.; Leiterer, C.; Fritzsche, W.; Gutsche, C.; Lysov, A.; Prost, W.; Tegude, F.-J.; Pertsch, T.; Tünnermann, A.; Christiansen, S. Far-Field Imaging for Direct Visualization of Light Interferences in GaAs Nanowires. *Nano Lett.* **2012**, *12*, 5412−5417.
(14) Dutto, F.; Raillon, C.; Schenk, K.; Radenovic, A. Nonlinear Optical Response in Single Alkaline Niobate Nanowires. *Nano Lett.* **2011**, *11*, 2517−2521.
(15) Sergeyev, A.; Geiss, R.; Solntsev, A. S.; Steinbrück, A.; Schrempel, F.; Kley, E.-B.; Pertsch, T.; Grange, R. Second-Harmonic Generation in Lithium Niobate Nanowires for Local Fluorescence Excitation. *Opt. Express* **2013**, *21*, 19012.
(16) Boyd, R. W. *Nonlinear Optics*, 2nd ed.; Academic Press: Amsterdam, 2003.
(17) Kim, E.; Steinbrück, A.; Buscaglia, M. T.; Buscaglia, V.; Pertsch, T.; Grange, R. Second-Harmonic Generation of Single $BaTiO_3$ Nanoparticles down to 22 nm Diameter. *ACS Nano* **2013**, *7*, 5343−5349.
(18) Richter, J.; Steinbrück, A.; Zilk, M.; Sergeyev, A.; Pertsch, T.; Tünnermann, A.; Grange, R. Core-Shell Potassium Niobate Nanowires for Enhanced Nonlinear Optical Effects. *Nanoscale* **2014**, *6*, 5200−5207.
(19) Casadei, A.; Pecora, E. F.; Trevino, J.; Forestiere, C.; Ru, D.; Russo-averchi, E.; Matteini, F.; Tutuncuoglu, G.; Heiss, M.; Fontcuberta, A.; Negro, L. D. Photonic − Plasmonic Coupling of GaAs Single Nanowires to Optical Nanoantennas. *Nano Lett.* **2014**, *14*, 2271−2278.
(20) Lehr, D.; Reinhold, J.; Thiele, I.; Hartung, H.; Dietrich, K.; Menzel, C.; Pertsch, T.; Kley, E.-B.; Tünnermann, A. Enhancing Second Harmonic Generation in Gold Nanoring Resonators Filled with Lithium Niobate. *Nano Lett.* **2015**, *15*, 1025−1030.
(21) Ducci, S.; Lanco, L.; Berger, V.; De Rossi, A.; Ortiz, V.; Calligaro, M. Continuous-Wave Second-Harmonic Generation in Modal Phase Matched Semiconductor Waveguides. *Appl. Phys. Lett.* **2004**, *84*, 2974.
(22) Wagner, S. J.; Holmes, B. M.; Younis, U.; Helmy, A. S.; Aitchison, J. S.; Hutchings, D. C. Continuous Wave Second-Harmonic Generation Using Domain-Disordered Quasi-Phase Matching Waveguides. *Appl. Phys. Lett.* **2009**, *94*, 151107.
(23) Xiong, C.; Pernice, W.; Ryu, K. K.; Schuck, C.; Fong, K. Y.; Palacios, T.; Tang, H. X. Integrated GaN Photonic Circuits on Silicon (100) for Second Harmonic Generation. *Opt. Express* **2011**, *19*, 10462−10470.
(24) Schiek, R.; Pertsch, T. Absolute Measurement of the Quadratic Nonlinear Susceptibility of Lithium Niobate in Waveguides. *Opt. Mater. Express* **2012**, *2*, 126−135.
(25) Moutzouris, K.; Venugopal Rao, S.; Ebrahimzadeh, M.; De Rossi, A.; Calligaro, M.; Ortiz, V.; Berger, V. Second-Harmonic Generation through Optimized Modal Phase Matching in Semiconductor Waveguides. *Appl. Phys. Lett.* **2003**, *83*, 620.
(26) Beckmann, T.; Linnenbank, H.; Steigerwald, H.; Sturman, B.; Haertle, D.; Buse, K.; Breunig, I. Highly Tunable Low-Threshold Optical Parametric Oscillation in Radially Poled Whispering Gallery Resonators. *Phys. Rev. Lett.* **2011**, *106*, 143903.
(27) Werner, C. S.; Beckmann, T.; Buse, K.; Breunig, I. Blue-Pumped Whispering Gallery Optical Parametric Oscillator. *Opt. Lett.* **2012**, *37*, 4224−4226.
(28) Fürst, J. U.; Strekalov, D. V.; Elser, D.; Lassen, M.; Andersen, U. L.; Marquardt, C.; Leuchs, G. Naturally Phase-Matched Second-Harmonic Generation in a Whispering-Gallery-Mode Resonator. *Phys. Rev. Lett.* **2010**, *104*, 153901.
(29) Yan, R.; Gargas, D.; Yang, P. Nanowire Photonics. *Nat. Photonics* **2009**, *3*, 569−576.
(30) Hartung, H.; Kley, E.-B.; Gischkat, T.; Schrempel, F.; Wesch, W.; Tünnermann, A. Ultra Thin High Index Contrast Photonic Crystal Slabs in Lithium Niobate. *Opt. Mater.* **2010**, *33*, 19−21.
(31) Palima, D.; Bañas, A. R.; Vizsnyiczai, G.; Kelemen, L.; Ormos, P.; Glückstad, J. Wave-Guided Optical Waveguides. *Opt. Express* **2012**, *20*, 2004−2014.
(32) Solntsev, A. S.; Sukhorukov, A. A.; Neshev, D. N.; Iliew, R.; Geiss, R.; Pertsch, T.; Kivshar, Y. S. Cascaded Third Harmonic Generation in Lithium Niobate Nanowaveguides. *Appl. Phys. Lett.* **2011**, *98*, 231110.
(33) Edwards, G. J.; Lawrence, M. A Temperature-Dependent Dispersion Equation for Congruently Grown Lithium Niobate. *Opt. Quantum Electron.* **1984**, *16*, 373−375.
(34) Snyder, A. W.; Love, J. *Optical Waveguide Theory*; Springer Science, 1983.
(35) Klein, A. E.; Janunts, N.; Steinert, M.; Tu, A.; Pertsch, T. Polarization-Resolved Near-Field Mapping of Plasmonic Aperture Emission by a Dual-SNOM System. *Nano Lett.* **2014**, *14*, 5010−5015.
(36) Johnson, J. C.; Yan, H. Q.; Schaller, R. D.; Petersen, P. B.; Yang, P. D.; Saykally, R. J. Near-Field Imaging of Nonlinear Optical Mixing in Single Zinc Oxide Nanowires. *Nano Lett.* **2002**, *2*, 279−283.

DOI: 10.1021/acsphotonics.5b00126
ACS Photonics 2015, 2, 687−691